· **N94- 30128**

Experimental Investigation of Possible Geomagnetic Feedback From Energetic (0.1 to 16 keV) Terrestrial O^+ Ions in the Magnetotail Current Sheet

O. W. Lennartsson, D. M. Klumpar, E. G. Shelley, and J. M. Quinn

Division of Research and Development, Lockheed Missiles and Space Company, Incorporated, Palo Alto, California

Data from energetic ion mass spectrometers on the ISEE 1 and AMPTE/CCE spacecraft are combined with geomagnetic and solar indices to investigate, in a statistical fashion, whether energized O^+ ions of terrestrial origin constitute a source of feedback which triggers or amplifies geomagnetic activity, as has been suggested in the literature, by contributing a destabilizing mass increase in the magnetotail current sheet. The ISEE 1 data (0.1–16 keV/e) provide in situ observations of the O^+ concentration in the central plasma sheet, inside of 23 R_E, during the rising and maximum phases of solar cycle 21, as well as inner magnetosphere data from same period. The CCE data (0.1–17 keV/e), taken during the subsequent solar minimum, all within 9 R_E, provide a reference for long-term variations in the magnetosphere O^+ content. Statistical correlations between the ion data and the indices, and between different indices, all point in the same direction: there is probably no feedback specific to the O^+ ions, in spite of the fact that they often contribute most of the ion mass density in the tail current sheet.

1. Introduction

Singly charged oxygen is a variable but usually substantial component of the magnetospheric plasmas at most energies [*Shelley et al.*, 1972; *Ghielmetti et al.*, 1978; *Balsiger et al.*, 1980; *Sharp et al.*, 1981; *Lundin et al.*, 1982; *Lennartsson and Shelley*, 1986; *Möbius et al.*, 1987; *Gloeckler and Hamilton*, 1987; *Chappell et al.*, 1987]. It is perhaps, besides H^+ and He^{++} ions, the most important ion component from a scientific point of view, for at least two reasons. One is its principal source, Earth's atmosphere [*Young et al.*, 1982; *Kremser et al.*, 1988], which makes it a unique measure of electrical solar-terrestrial interactions. This is the one aspect that has received the closest attention in the literature so far. Another reason, however, is the large mass or mass per charge of the O^+ ions compared to that of the H^+ ions. A mere 10% admixture of O^+ ions in an otherwise pure H^+ population will more than double the mass density of the plasma, even though the number density and charge density remain almost the same. And a 50-50 mixture of O^+ and H^+ ions, often reached in the inner magnetosphere [*Lennartsson and Sharp*, 1982] and sometimes in the central plasma sheet as far out as 20 R_E [*Peterson et al.*, 1981], will have almost an order of magnitude greater mass density than the corresponding number of only H^+ ions. This property of the O^+ component may have significant consequences for the plasma dynamics; it certainly has for hydromagnetic wave propagation [e.g., *Singer et al.*, 1979].

Although the energetic (keV) O^+ ions observed in the near-equatorial magnetosphere are commonly perceived to be a product of geomagnetic storm or substorm activity, a good case has been made for feedback effects as well [e.g., *Baker et al.*, 1982, 1985; *Delcourt et al.*, 1989; *Daglis et al.*, 1990, 1991; *Moore and Delcourt*, 1992; *Swift*, 1992]. *Baker et al.* [1982] argued that the addition of such O^+ ions in the tail current sheet, after the onset of a substorm, will have a destabilizing effect on this sheet, especially at $-15 R_E < $ GSM $X < -10 R_E$, the reason being that the large mass per charge of the O^+ ions may cause the sheet ion population to become increasingly demagnitized and therefore more susceptible to ion tearing mode instabilities. This course of reasoning allows for the initial increase in the tail O^+ population, after a period of geomagnetic quiescence, to be induced entirely by external forces, but it suggests that the increased concentration of O^+ ions will promote consequent substorm onsets, thereby prolonging and strengthening many active periods.

One observational fact that may seem to fit with that kind of scenario is the tendency of very strong substorms, those with a peak AE index of 1000 nT or greater, to occur in clusters during extended periods (often a day or longer) of elevated AE (see, for example, *Kamei and Maeda* [1981] and *Baker et al.* [1985]). On the other hand, more long-term records of geomagnetic and solar activity, covering several years, may not seem to fit the same trend, because the energetic O^+ population has been found to vary substantially in density over the course of a solar cycle without causing a parallel long-term variation of geomagnetic activity [*Young et al.*, 1982; *Yau et al.*, 1985; *Lennartsson*, 1989]. None of the long-term studies of O^+ ions has been specifically directed towards the feedback aspect, however, so there is still room for doubt either way.

This study attempts to clarify, to the extent possible with statistical methods, whether there is a geomagnetic feedback specific to the O^+ ions, by comparing extensive sets of near-equatorial ion composition data with common geomagnetic and solar activity indices. In order to utilize the long-term observations now available from similar experiments, data obtained during the rising and maximum phases of solar cycle 21 by a mass spectrometer on the International Sun-Earth Explorer (ISEE 1) spacecraft are intercompared with data obtained near the end of the same cycle, at the minimum phase, by the same kind of spectrometer on the Charge Composition Explorer (CCE) spacecraft of the Ac-

PRECEDING PAGE BLANK NOT FILMED

tive Magnetosphere Particle Tracer Explorer (AMPTE) mission.

The focus of this study is on the consequences, if any, of increasing the average mass per ion in the central plasma sheet by adding O^+ ions, or replacing H^+ ions with O^+ ions. It is recognized that the O^+ ions, along with other ions of terrestrial origin, energetic or not, must have some role in magnetosphere dynamics simply by contributing a positive plasma component but that aspect is more complex and does not necessarily distinguish the O^+ as a species. It is the exceptional capability of the O^+ to enhance the plasma mass density that is of principal interest here.

2. INSTRUMENTATION

The ISEE 1 spacecraft (along with the ISEE 2) was launched on October 22, 1977, into an orbit with apogee at almost 23 R_E (geocentric), perigee at ~300 km altitude, an inclination of 29°, and an orbital period of 57 hours. It was placed in a spinning mode with the axis nearly perpendicular to the solar ecliptic plane and with a period of approximately 3 s. The AMPTE CCE, one in a stack of three separate spacecraft, was launched on August 16, 1984, and directed into a very nearly equatorial orbit with apogee at almost 9 R_E, perigee at ~1000 km altitude, an inclination of less than 5°, and an orbital period of 15.6 hours. The AMPTE CCE is also in a spinning mode, but its spin axis is parallel to Earth's equatorial plane, pointing some 10° to 30° from the Sun direction, and its spin period is 6 s.

The Lockheed ion composition experiments flown on ISEE 1 and AMPTE/CCE are two of a family of instruments using the same type of ion optics and covering nearly the same range of energies (0 eV/e to ~17 keV/e) which have also been flown on GEOS 1 and 2 and on DE 1 [*Shelley et al.*, 1978, 1985]. The ISEE 1 instrument consists of two nearly identical mass spectrometers with the respective fields of view centered 5° above and 5° below the spin plane, that is about 5° above and below the solar ecliptic plane. Data used in this study are from one of these, the one looking below the spin plane. The CCE instrument has a single mass spectrometer with the field of view centered in the spin plane, which in that case is roughly perpendicular to the solar ecliptic plane, oriented somewhat like the GSE *Y-Z* plane. Each field of view is ~10° wide along the spin plane, and some 10° to 50° wide transverse to this plane, being the widest at the low-energy end (due to preacceleration) and gradually decreasing toward 10° with increasing energy. Information on the instantaneous pitch angles (at center of field of view) is provided by the ISEE 1 fluxgate magnetometer [*Russell*, 1978] and the AMPTE CCE Magnetic Field Experiment [*Potemra et al.*, 1985].

Each spectrometer consists of an electrostatic analyzer to select energy per charge, followed by a combined electrostatic and magnetic analyzer to select mass per charge. Both analyzer sections have particle detectors, so at each energy setting the experiments provide both the total ion flux and the partial flux at a selected mass per charge. On ISEE 1 each combination of energy and mass is maintained for at least 1/16 s in high telemetry bit rate and 1/4 s in low (normal) bit rate, on CCE the corresponding time is 1/32 s. Different combinations are stepped through in a cyclic fashion according to various patterns controlled by a random access memory which is programmable from the ground. The ISEE

1 patterns, or "modes," used inside the magnetosphere usually require from 2 to 17 min to complete. Most commonly used CCE patterns require ~2 min per cycle. The mass selections include one that blocks all ions from reaching the second detector, allowing intermittent measurements of the noise associated with penetrating radiation. These measurements are later used to correct the count rates of mass analyzed ions.

The maximum energy range is 0 eV/e (or spacecraft potential) to 17.9 keV/e, divided into 32 contiguous channels, although only a subset of these may be used in a given mode (typically only 15 channels on CCE). The lowest channel, from 0 eV/e to ~100 eV/e, is normally limited to energies above 10 eV/e on ISEE 1 and above 30 eV/e on CCE by an RPA (retarding potential analyzer) in the entrance. That same RPA is used to provide "cold plasma" data from 0 to 100 eV/e (retarding within the lowest channel) during part of some measurement cycles. Because of measurement uncertainties associated with spacecraft charging and plasma convection, the lowest energy channel is treated separately when calculating velocity moments. Data from this channel are not included in the statistical material here but are discussed briefly in a separate section. In the case of ISEE 1, data from the highest-energy channel (above 16 keV/e) are also excluded from moment calculations, because of a slight variation over time of the mass response in that channel. Whenever the energy scans have left some intermediate energy channels unsampled, an interpolation procedure has been employed, assuming a linear variation of the differential flux. Given these considerations, and given the numerical procedures used for weighting and summing counts from the various energy channels, the velocity moments displayed in the following figures correspond to an energy range of ~100 eV/e to 16 keV/e for ISEE 1 and 100 eV/e to 17 keV/e for AMPTE/CCE.

3. DATA FORMATS

This study is the first extensive application of two archival data sets recently completed for NASA's Explorer Project. The formats of these data are designed to be a compact representation, with roughly the same time resolution as that provided by the instrument energy-mass scan cycle. Although these data sets include various spectral information, only the files containing velocity moments have been used here.

The ISEE 1 data files contain separate velocity moments for the four principal ion species, H^+, He^{++}, He^+, and O^+, calculated once each energy-mass scan cycle, using two different methods to be explained below. Each moment has a statistical uncertainty (standard deviation) assigned to it, calculated with standard formulas for error propagation assuming Poisson counting statistics and including the uncertainty in background subtraction. In addition, there are velocity moments for "total ions," based on the total ion count rate in the electrostatic analyzer and assuming that this rate is due entirely to H^+ ions. These moments are calculated once per energy scan, providing a time resolution of a couple of minutes or better, and usually have nearly continuous time coverage. The reason for including "total" moments here is to help separate mass-resolved moments taken in different plasma regimes (see next section).

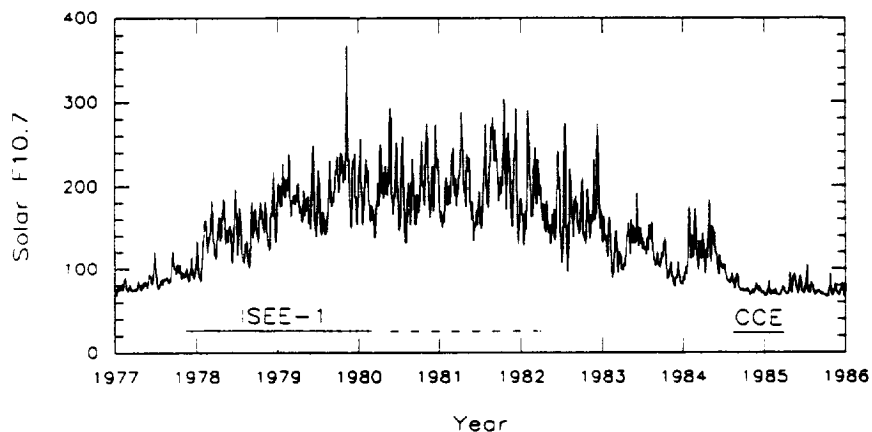To calculate full three-dimensional velocity moments from

Fig. 1. Time ranges of available ion composition data in relation to solar activity. Only the solid line (archived) portion of the ISEE 1 data is used here (years labeled at beginning).

the raw ISEE 1 data, the ion fluxes measured within the near-ecliptic field of view have been extrapolated to other angles using either of two sets of approximating assumptions:

1. The principal ion flow is parallel to the solar ecliptic plane and the ion fluxes have rotational symmetry around the flow vector, regardless of the magnetic field orientation. The direction of the flow vector within this plane is determined by the measured flow within the instrument field of view. The single angular variable in this case is divided among 12 30° spin-angle bins, roughly approximating the inherent angular resolution of the ISEE 1 instrument in normal low-bit-rate operation.

2. Fluxes are gyrotropic (independent of gyration angle) over the sampled range of pitch angles, and isotropic outside of this range, maintaining the values measured at the smallest and largest pitch angles, respectively. The pitch angles are divided among nine 20° bins. This assumption is only applied to number densities, mean energies, parallel and perpendicular to the magnetic field, and energy densities. It ignores any net bulk flow perpendicular to the magnetic field.

The two sets of assumptions typically yield about the same number densities and total energy densities, within statistical uncertainties, except for cases of substantial ecliptic ion drift across the magnetic field (substantial when compared to thermal velocities), when 1 appears to provide more accurate values, especially for number densities. This has been verified by comparing the ion densities with electron densities derived from ISEE 1 and 2 wave experiments on several occasions. Although the drift direction in 1 is determined from average fluxes in 30° wide bins, the weighting involved in the integrations usually provides an accuracy much better than 30°. For simplicity, the ISEE 1 number densities illustrated here are those derived from 1 when referring to the magnetotail (plasma sheet) and from 2 when referring to the inner magnetosphere (for comparison with CCE densities).

The AMPTE/CCE moment files use a common integration time of 6.4 minutes for both the mass resolved data and the total ion data. The CCE velocity moments have all been calculated according to approximation 2 above, including a standard deviation for each moment, except that the counts were initially separated between the right and left side of the magnetic field direction, in order to allow a cross-B velocity

to be calculated (along with a parallel velocity). Because of the attitude and orbit of the spacecraft, the CCE instrument normally samples fluxes along the magnetic field direction. In addition to the H⁺, He⁺⁺, He⁺, and O⁺ ions these files also include O⁺⁺ ions. It is clear from these data that the O⁺⁺ ions, as was assumed during the preparation of the ISEE 1 files, are generally much less abundant than the O⁺ ions at these energies, typically by 1 to 2 orders of magnitude (see also Young et al. [1982]). The same appears to hold at higher energies as well, according to data from the CHEM experiment on AMPTE/CCE [Kremser et al., 1988].

4. DATA SELECTION

The time coverage of the ISEE 1 and AMPTE/CCE data sets through solar cycle 21 is illustrated in Figure 1, along with the daily index of 10.7-cm wavelength solar radio flux. This index is commonly used as a proxy for the solar extreme ultraviolet (EUV) radiation [Hinteregger, 1981] and is therefore an indirect measure of the solar radiant effects on the terrestrial O⁺ source [e.g., Young et al., 1982, and references therein]. Figure 1 shows the reason for intercomparing the two data sets; the ISEE 1 set was acquired during strongly varying solar activity, including the peak, the CCE set during weak and extremely steady solar activity. The significance of this will be clarified later.

Of all the ISEE 1 data available, only three subsets have been used here, one obtained in the central plasma sheet, the other two in the inner magnetosphere, in the same spatial region as the CCE data. The spatial distribution of the plasma sheet samplings is illustrated in Figure 2 in GSM coordinates, with each point representing one instrument energy-mass cycle. The samplings are all from geocentric distances beyond 10 R_E and have been further limited to -10 $R_E < \text{GSM } Y < 10$ R_E and GSM $X < -5$ R_E. The main reason for choosing this particular region is that the plasma sheet O⁺ density has been found to have a rather broad maximum within 10 R_E of either side of local midnight during periods of hourly $AE > 200$ nT (see Figure 7d of Lennartsson and Shelley [1986]).

The central plasma sheet has been defined by the following conditions:

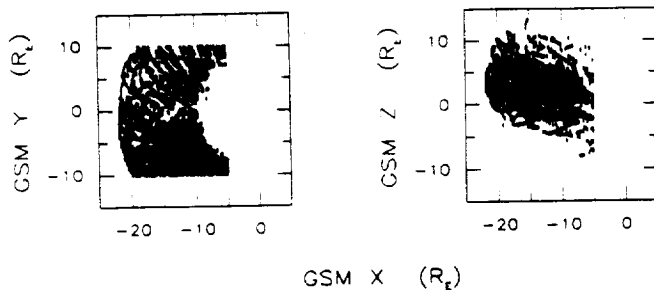1. The sum of the H⁺, He⁺⁺, He⁺, and O⁺ densities is at least 0.1 cm⁻³.

Fig. 2.   Spatial extent of selected plasma sheet data set (ISEE 1) in Geocentric Solar Magnetospheric (GSM) coordinates.

2. The plasma beta value produced by these same ions is at least 0.1.

3. The multiple densities derived from the total ion count rates during the course of each energy-mass scan cycle, assuming only H^+ ions (see previous section), are all at least $0.05 \, cm^{-3}$.

These conditions differ slightly from those used by *Lennartsson and Shelley* [1986] but lead to essentially the same selection, given the spatial constraints. The present data set is further constrained by the requirement that concurrent AE indices be available, resulting in the exclusion of samplings from 1977 (see *Kamei and Maeda* [1981], and subsequent data books). The resulting number of samples is 4056 (~1000 hours).

For this study the CCE samplings have first been binned and averaged into a time-space matrix of 1 hour UT by 1 hour MLT by one dipole L unit, in order to make the set more compact. The spatial distribution of the elements (average coordinates) is illustrated in Figure 3 in SM coordinates (same as GSM, except for a rotation around the Y axis to make the Z axis equal to the northward dipole axis). The samplings have been limited to $L > 6$ in order to ensure that the ion composition is controlled by the particle sources rather than by charge exchange decay [*Lennartsson and Sharp*, 1982]. In addition, the samplings have been confined to the inside of the magnetopause, by elimination of data that might be interpreted as magnetosheath or solar wind (based in part on total moments). The reason for dividing the data by year is that AE indices, at this writing, are not available on magnetic tape for 1985. The set is made up of 7998 individual 6.4-min samplings from 1984, and 8211 such
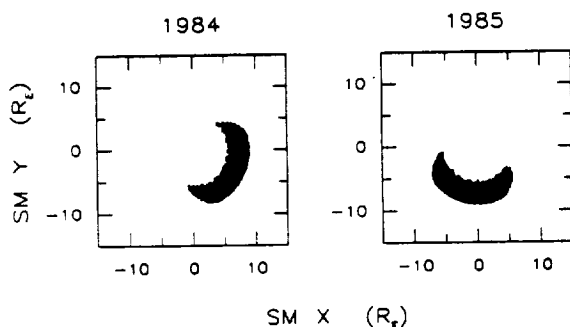

Fig. 3.   Spatial extent of selected CCE data sets in Solar Magnetic (SM) coordinates. These extend in geomagnetic latitude from −16° to +12°. Equivalent regions are used for ISEE 1 data as well (see text).

samplings from 1985, binned and averaged into 1732 and 1728 matrix elements, respectively.

The two spatial regions thus defined by the CCE data have in turn been used to select two "inner magnetosphere" sets of ISEE 1 data as well (similarly excluding magnetosheath and solar wind). The resulting number of samples in these ISEE 1 sets is 581 (corresponding to 1984 CCE set) and 693 (1985 CCE set).

5.   STATISTICAL RESULTS

Whether auroral substorms, as defined by enhancements in the AE index, for instance, are triggered by an increasing concentration of O^+ ions in the tail current sheet [e.g., *Baker et al.*, 1982], or always start independently of the O^+, may seem to be a simple question of timing. The answer is not readily found by studying individual events, however, because the O^+ data from within the plasma sheet are rather spotty during active periods, due to plasma sheet motion and thinning, and the substorm activity is often recurring too rapidly to allow a unique association between enhancements in the AE and in the O^+ density. The only firm conclusion that can be drawn from previous event studies is that there are numerous cases where the ISEE 1 is in the central plasma sheet at a substorm expansion onset and does not observe a large concentration of O^+ (>10%) until after onset (R. D. Sharp, unpublished manuscript, 1982; see also *Baker et al.* [1985]). Hence we have had reasons to believe that substorms can occur before the O^+ density is enhanced in the tail, but we still do not know whether they occur more easily if the O^+ density is already high, or if they are stronger in that case.

5.1.   Relative Timing

As a first step in addressing this question, the entire set of ISEE 1 plasma sheet data, as defined above (see Figure 2), was scoured for evidence that the O^+/H^+ density ratio might sometimes undergo a significant increase shortly before such an increase takes place in the AE index. Several different approaches were tried, using different definitions of "significant increase" and "shortly before." The result was essentially negative; there was no clear evidence that any increment in the AE could be uniquely associated with a preceding, or even simultaneous, increase in the O^+/H^+ ratio, and this was due in part to the difficulties already mentioned. One approach, for example, was to use hourly AE indices and pose the following problem:

Find each sampling with an O^+/H^+ ratio greater than 30%, which is preceded by at least a 3-hour period of samplings with O^+/H^+ consistently less than 20%, allowing no more than 60 min for data gaps during that period, and check whether the concurrent or succeeding hourly AE is greater, by any amount, than the preceding 3-hour average AE. The result: No case of a succeeding increase in the hourly AE, but one case of a concurrent increase. In that one case the 1-min AE indices were examined next, and the AE proved to increase ahead of the increase in the O^+/H^+ ratio.

5.2.   Correlation Between AE and Average Ion Mass in Plasma Sheet

Figure 4 shows a purely statistical approach, where each plasma sheet sampling is represented by its linearly averaged

N=4056

hourly AE   (nT)

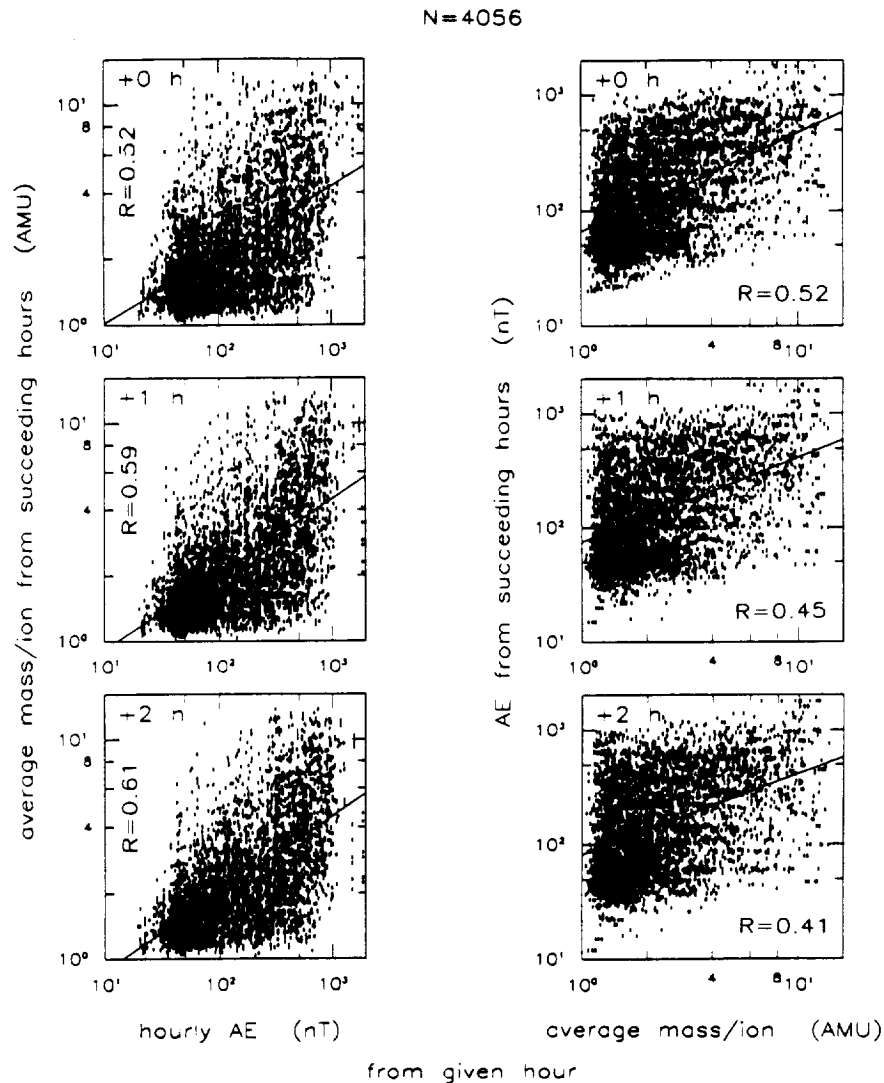average mass/ion   (AMU)

from given hour

Fig. 4.   Scatterplots of average ion mass in plasma sheet versus hourly AE (left) and vice versa (right). The top panels compare AE readings and mass samplings from same hour, the lower panels compare AE or mass with mass and AE from the first (middle) and second (bottom) succeeding hour. The regression lines in this and following figures have a correlation coefficient as indicated by parameter R. The parameter N indicates the number of data points in each panel.

ion mass, weighted by the respective densities of H$^+$, He^{++}, He$^+$, and O$^+$ ions (thus having a range of 1.0 to 16.0 amu), and is associated with hourly AE indices from the same (top panels) or adjacent hours. Because the He^{++} ions are always in minority here (almost always less than 10% of total number density), the average mass is also approximately the average mass per charge, which may be the physically more significant quantity (or mass divided by the square of the charge). This mass, whether associated with ion or charge, is not expected to be significantly defective by not including O^{++} ions (see end of section 3).

In the left panels of Figure 4 the average mass is treated as a function of the hourly AE index, allowing up to 2 hours delay from each AE reading to the plasma sheet sampling. The slanted straight line in each panel is the linear least squares fit of log (mass) versus log (AE). The reason for using a linear fit here is that when the AE is binned, rather than scattered, the logarithm of the average mass in each AE bin is approximately a linear function of the logarithm of AE

(not shown). The correlation coefficient, denoted by the letter R, is significant in each case, given the large number of points (4056). The generally greater mass/ion during active times is due to a combination of increasing O$^+$ density and decreasing H$^+$ and He^{++} densities [see Lennartsson and Shelley, 1986]. The He$^+$ ions contribute a negligible density in the central plasma sheet at most times. It can be seen that the correlation is somewhat better with a 2-hour delay than with a shorter delay, or no delay. The correlation with a 2-hour delay is in fact at its maximum; it declines again with longer delays, reaching a value of $R = 0.45$ with a 5-hour delay, for instance (not illustrated).

In the right panels of Figure 4 the AE index is similarly treated as a function of the average mass, using the same set of plasma sheet samplings. In this case the correlation coefficient declines monotonically with increasing delay, reaching $R = 0.45$ already with a 1-hour delay (and $R = 0.31$ with a 5-hour delay). Clearly, the AE is less well correlated with preceding values of the average ion mass

TABLE 1. Autocorrelation of Log (Hourly AE) in 1978–1979
(N = 17520)

Lag Time, hours	Correlation Coefficient
1	0.87
2	0.70
3	0.61
4	0.55
5	0.51
6	0.46

than vice versa. Note also that the regression line in the top right panel is different from the corresponding line in the top left panel, even though the two correlation coefficients are the same (by definition).

Figure 4 displays all plasma sheet samplings corresponding to Figure 2, including both dawn and dusk halves. It may be true that conditions in the dusk half are usually the most relevant to substorm onset, as argued by *Baker et al.* [1982], but these ion composition data show no significant asymmetry between dusk and dawn and do not justify limiting the statistical material to the dusk side only. By including the dawn half it is possible to admit more samplings from early 1978 and early 1980 and thus cover a wider range of solar surface activity (see Figure 1). This is a desirable objective in the next section. It may suffice to mention that if the scatterplots of Figure 4 are limited to the dusk half, where there are 1366 samplings, the least squares fits are virtually identical to those in Figure 4, and the correlation coefficients differ by at most 0.02.

It is quite possible that the nonzero correlation of the AE with the preceding values of the average ion mass in the right panels of Figure 4, with 1- and 2-hour delays, is purely accidental, because the AE has a very high degree of autocorrelation over long periods of time. This is illustrated by Table 1, which lists the correlation coefficients for hourly AE values taken from one to six hours apart during 1978 and 1979 (17520 hours). As can be seen, the AE at any one time is still better correlated with the AE from as much as 6 hours earlier than it is with the average ion mass during the immediately preceding hour.

5.3. Solar Cycle Effects

Figure 5 relates the average ion mass in the central plasma sheet to solar surface activity, as measured by the $F_{10.7}$, as well as geomagnetic activity. The ion mass samplings in the left panel are from geomagnetically "quiet" times, defined by requiring that the hourly AE index be consistently less than 100 nT over a 3-hour period, where the middle hour contains the mass sampling. The right panel has samplings from "disturbed" times, similarly defined by hourly AE indices being consistently greater than 200 nT over that same 3-hour period. By considering AE indices taken both before and after the mass sampling it is ensured that no bias is placed on the causal relationship between the AE and the ion mass, although the strong autocorrelation of the AE index makes the precise timing less important (see Table 1). In any case the average ion mass is found to increase with increasing solar activity, regardless of substorm activity level, and this is mainly a consequence of an increasing O$^+$ density (see also *Young et al.* [1982] and *Lennartsson* [1989]). The regression lines are again based on log (mass), because a logarithmic y scale and a linear x scale provide a roughly linear dependence when data points are binned in x and averaged in y (not shown).

Although the correlation coefficient is only about 0.3 in both panels of Figure 5, the large number of data points makes it significant. It can be seen, by using standard statistical tests [*Bevington*, 1969, pp. 119–127; *Press et al.*, 1986, pp. 484–487], that the probability of having no actual correlation between the ion mass and the solar activity is negligible (less than 10^{-8}). Essentially, the same statistical results are reached even if the samplings are limited to the dusk half of the plasma sheet, thereby reducing the number of data points as well as the range of $F_{10.7}$. In that case, N = 339 and R = 0.25 in the left panel (AE < 100 nT) and N = 348 and R = 0.36 in the right panel (AE > 200 nT), and the respective regression lines remain identical within one standard deviation of either the slope or the vertical location.

By contrast, the substorm activity, as measured by the AE or Kp indices, does not increase with increasing solar surface activity during this time period, neither in terms of frequency of substorm onsets nor in terms of peak ampli-
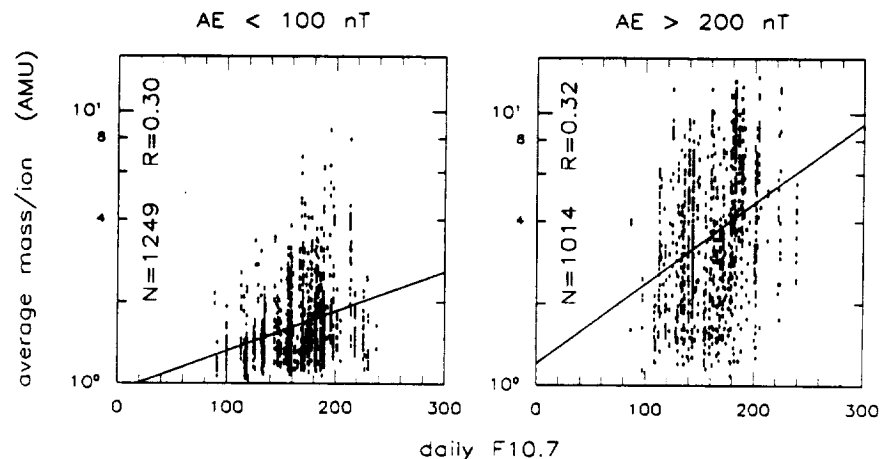

Fig. 5. Comparison of ion mass in plasma sheet with the Ottawa daily $F_{10.7}$ index (solar radio flux) during geomagnetically (left) quiet and (right) disturbed conditions (see text for selection of AE). The ion samplings have been ordered by Ottawa local time here, rather than by the usual universal time.
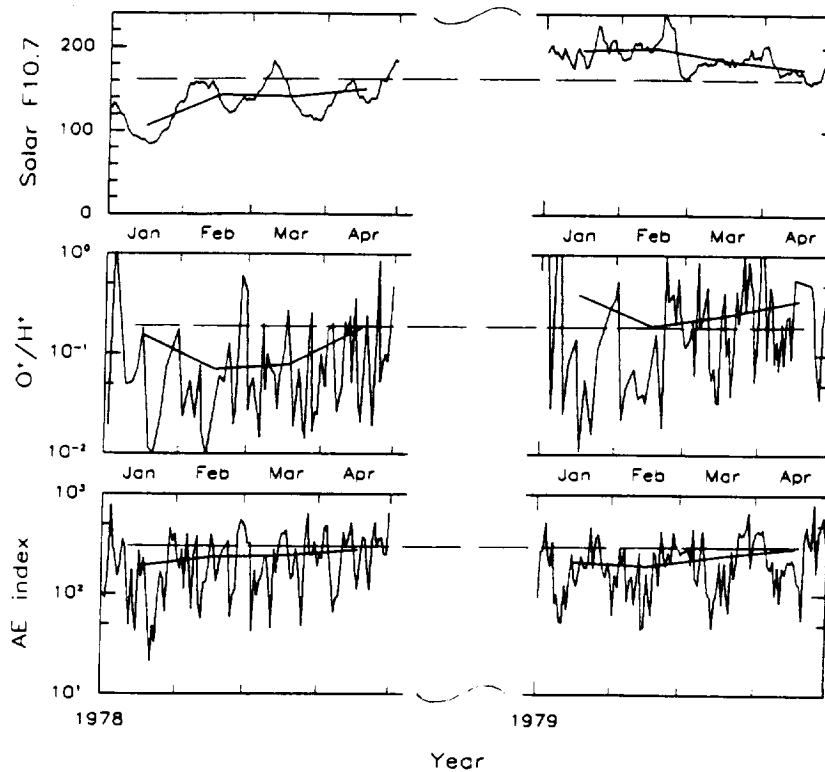
Fig. 6. (Top) Daily (jagged line) and monthly $F_{10.7}$; (middle) daily and monthly averaged plasma sheet O$^+$/H$^+$ density ratio; (bottom) daily and monthly averaged AE index. The dashed horizontal lines are for visual reference.

tude. This is partly illustrated for the AE index by Figure 6, which covers two 4-month intervals with similar ISEE 1 samplings of the plasma sheet (as defined in Figure 2), one in 1978, the other in 1979. The daily solar $F_{10.7}$ (top panel), and presumably also the concurrent EUV flux, is almost consistently higher in the later interval, resulting in a generally greater O$^+$/H$^+$ density ratio in the central plasma sheet, also represented by "daily" numbers here (middle panel), obtained by averaging all available samplings each day. These trends are still more distinct in terms of monthly averages, shown here by points centered on each month and connected by straight lines. However, the AE index (bottom panel) shows no signs of increasing from 1978 to 1979, neither as a daily nor as a monthly average (see also Figure 3 in the work by Young et al. [1982]). As far as the frequency of substorm onsets is concerned, a visual inspection of 1-min AE records (see Kamei and Maeda [1981] and subsequent data books) reveals no obvious increase from 1978 to 1979 (not illustrated here).

It may be argued that Figure 6 does show some change from 1978 to 1979 in the daily averaged AE index, since in 1979, but not in 1978, the AE appears to be modulated at a rate resembling the solar rotation period, which ranges from 25 to 36 days, depending on latitude and physical feature [Hansen et al., 1969, and references therein]. This is probably not caused by a solar-induced periodicity in the O$^+$ density, however, since the $F_{10.7}$ index is much less periodic in 1979 than in 1978. The fact that the O$^+$/H$^+$ ratio in Figure 6 does not show a clear solar rotation modulation, not even in 1978, can probably be ascribed to the rapidly varying sampling conditions, including the spacecraft motion along the orbit (at least 7 R_E per day) and the orbital drift relative to the tail ($\sim$12 R_E per month at apogee).

Returning to Figure 1, it is clear that the $F_{10.7}$ index continues to have strong oscillations for the next couple of years, including those caused by solar rotation, but it does not begin to change in a more long-term fashion again until 1983, when it starts declining, and it is not until the second half of 1984 that it reaches a low and steady level, coincident with the AMPTE/CCE data interval. At this time the $F_{10.7}$ is very close to its minimum daily (65.8 on October 8, 1985) and monthly values (69.4 in September 1986, which is the canonical end of solar cycle 21). Accordingly, the CCE data set should have substantially lower O$^+$ concentrations than the ISEE 1 set, even if the ISEE 1 set is averaged over most of the rising phase (to improve statistics). The CCE data contain no samplings from the plasma sheet region shown in Figure 2, but it is known from the ISEE 1 data that O$^+$ ions in the inner magnetosphere (R < 10 R_E) have virtually the same response to the $F_{10.7}$ index as do the plasma sheet O$^+$ ions [Lennartsson, 1989]. Hence, if the CCE data do show much lower O$^+$/H$^+$ ratios than do the ISEE 1 data, given the same inner magnetosphere sampling region for both sets, then it is fair to assume that the plasma sheet O$^+$/H$^+$ ratios are also substantially reduced at solar minimum (reversing the time sequence in Figure 6).

Figure 7 shows one kind of comparison between ISEE 1 and CCE data within the bounds of available AE indices. In this case each ion sampling has been associated with the average of 6 successive hourly AE indices, the last of which is concurrent. There is no special reason for choosing a 6-hour period per se, but the statistical correlation is somewhat better when an average of several hourly AE values is used rather than some single preceding value. Using preceding rather than succeeding AE values here seems intuitively
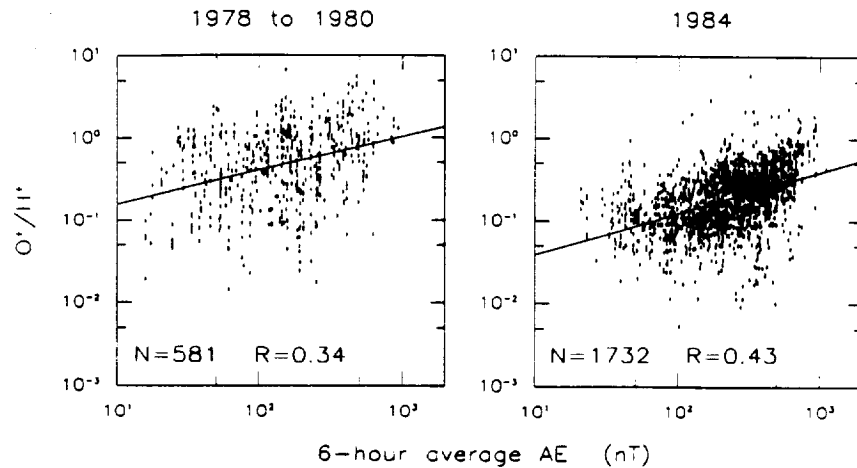
Fig. 7. Comparison of O^+/H^+ density ratio in the equatorial magnetosphere (dawn to noon; see left panel of Figure 3) with the preceding 6-hour average AE index during (left) rising-to-maximum and (right) minimum solar activity. The grand average AE during the two data sampling intervals was (left) 203 ± 7 nT and (right) 280 ± 5 nT.

right [cf. *Strangeway and Johnson*, 1984], regardless of the role of O^+ ions in the plasma sheet, and that choice is also justified by improved correlation.

Figure 7 confirms that the O^+/H^+ ratio has declined quite substantially in late 1984, near solar minimum, as compared to typical values during the rising phase of 1978 to early 1980. Even though the two instruments have different pitch angle coverage in this region of space (sections 2 and 3), the difference in the O^+/H^+ ratio between the left (ISEE 1) and right (CCE) panels is quite consistent with a time reversal of the results obtained between 1978 and 1980 at geosynchronous altitude ($L \approx 6.6$) by the GEOS 2 instrument (measuring nearly perpendicular to the magnetic field). If a median $F_{10.7}$ of 175 is assigned to the ISEE 1 data [*Lennartsson*, 1989] and an $F_{10.7}$ of 70 to the CCE data (Figure 1), the logarithmic regression formula in Table 3b of *Young et al.* [1982] predicts a reduction in the ratio by a factor of ~3.5 in 1984 for geomagnetically quiet conditions. Comparing the two regression lines in Figure 7 at low AE yields a somewhat larger reduction by a factor of 4.1, but the difference is probably within the margins of error, considering that the ISEE 1 data in Figure 7 span such a wide range of $F_{10.7}$. In any case there is a clear downward displacement of the regression line in 1984, and there is relatively less scatter about this line, resulting in a higher correlation coefficient. The improved correlation with the AE index is consistent with the strongly reduced fluctuations in the daily $F_{10.7}$ index (Figure 1), provided the O^+/H^+ ratio, as implied by Figure 5, depends not only on long-term but also on day-to-day variations in the solar irradiation.

In spite of this substantial long-term reduction in the O^+/H^+ ratio, there is no corresponding reduction in substorm activity. Instead, there is a modest but statistically significant increase over the same time period, as measured by for instance daily averages of the AE index (see *Kamei and Maeda* [1981], and subsequent data books). This trend is reflected in Figure 7 by the different grand average AE values during the two intervals of ion sampling (203 nT in the ISEE 1 interval, 280 nT in the CCE interval, the two mean values differing by more than ten times the standard deviation of either mean).

These opposing effects are even more clearly demon-

strated by means of the Kp index, which allows all of the CCE data to be used (and more than twice as much of the ISEE 1 data; see end of section 4). In Figure 8 each ion sampling has been associated with the linear average of the concurrent and the two immediately preceding Kp indices, assigning the numerical values +1/3 and −1/3 to the graduating plus and minus symbols on the Kp index. The resulting 9-hour average Kp has been binned, as shown, and the density ratios have been averaged within each bin. The grand average Kp during the two sets of ion samplings is indicated in the respective panel, in conventional notation, and further described in the caption. When expressed in decimal numbers, the two mean values differ by 50 times the standard deviation of either mean.

To place these results in a broader perspective, the hourly and daily averaged AE for all of 1978 through 1984 have been plotted versus the daily $F_{10.7}$ in Figure 9 (except for 1 day of missing $F_{10.7}$ index in 1983). Although small in magnitude, the resulting correlation coefficients are statistically significant, considering the large number of points [*Bevington*, 1969, pp. 119–127; *Press et al.*, 1986, pp. 484–487]. The fact that the two regression lines have almost exactly the same slope (same within two decimal places), even though the two sets of data points differ in size by a factor of 24, makes it almost certain that the correlation is real and not merely due to numerical rounding errors. The negative sign of the correlation is consistent, in a superficial sense, with the long-term anticorrelation just found between the O^+/H^+ ratio and the AE (Figure 7) and Kp (Figure 8), since the O^+ density is positively correlated with the $F_{10.7}$ (Figure 5; see also *Young et al.* [1982] and *Lennartsson* [1989]). This does not by itself imply a physical relationship between the AE and the $F_{10.7}$, however, because Figure 9 spans the better part of a solar cycle, and the important physical parameter may be solar cycle phase, or simply time. Indeed, if the AE is sorted by the $F_{10.7}$ on a year-by-year basis, the correlation does not even show a persistent sign. This is illustrated by Table 2.

5.4. Effects of Including Lowest Energy Channel

The possible role of ions with energies below 100 eV/e is primarily an issue with data obtained in situ, that is the ISEE
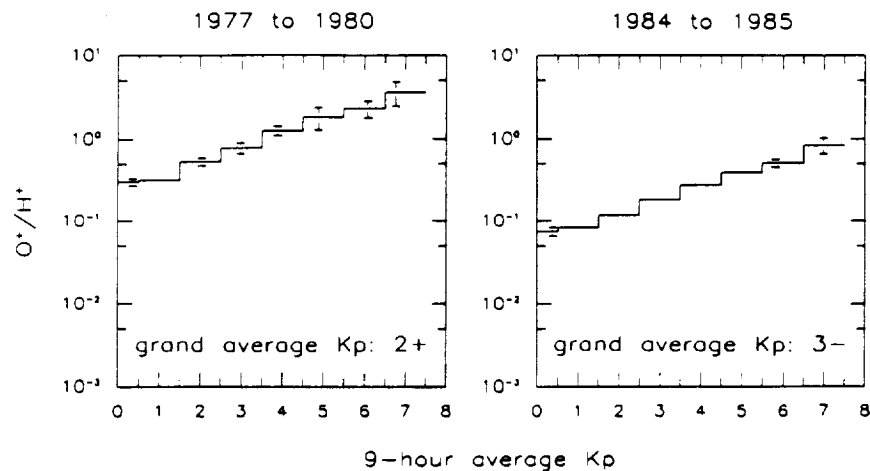
Fig. 8.   Averages of same ratio as a function of the preceding 9-hour average Kp index, covering similar phases of the solar cycle, but including a larger spatial region (left and right panels of Figure 3 combined). The error bars indicate the standard deviation (plus and minus) of the average ratio in each Kp-bin, and is drawn at the average Kp within the bin (when greater than the line width). The grand average Kp in each panel represents an actual decimal number of (left) 2.26 ± 0.01 and (right; see text) 2.76 ± 0.01.

1 plasma sheet data (Figure 2). The nominal range of 10–100 eV/e, not including variable RPA settings, has been measured in ~90% of the 4056 plasma sheet samplings, and these measurements almost always cover all 12 spin angle sectors at least once.

Count rates in this single energy channel have been converted to partial ion number densities assuming rotational symmetry of the ion flux around the same flow vector used for the main velocity moments (assumption 1 in section 3). This average flow vector, one for each ion species, has been based on count rates in all the other energy channels (except the highest one) and does not always approximate the true flow direction of the 10- to 100-eV/e ions. This can be a significant problem when the flux of low-energy ions is strongly focused in spin angle, in which case an error in the axis of symmetry leads to exaggerated densities.

Adding these partial densities, when measured, to the main densities has almost no effect on the statistical picture, however. In most samplings from the central plasma sheet the O⁺ and He⁺ densities are increased by less than 15%

and the H⁺ and He⁺⁺ densities by less than 5%. Table 3 shows the average increases. Part of the reason for these modest numbers may be that the low-energy cutoff is actually higher than 10 eV/e in much of the plasma sheet data, perhaps more typically between 10 and 20 eV/e, because of positive spacecraft charging associated with photo electron emission (see Figure 1 of Mozer et al. [1983]).

When Figures 4 and 5 are reproduced with the lowest-energy channel included (not shown), the new scatter patterns are virtually identical to the old ones. There is a barely perceptible flattening of the regression lines, corresponding quantitatively to a change in the third decimal place of the respective slopes. This flattening is accompanied by a slight reduction in the correlation coefficients as well, and this is again limited to the third decimal place in all cases but the left panel of Figure 5, where R is reduced to 0.28. Although very small, the reductions in the slopes and correlation coefficients of each regression line both indicate disordering. Hence, as far as the ion composition is concerned, adding the 10- to 100-eV/e partial densities in the central plasma
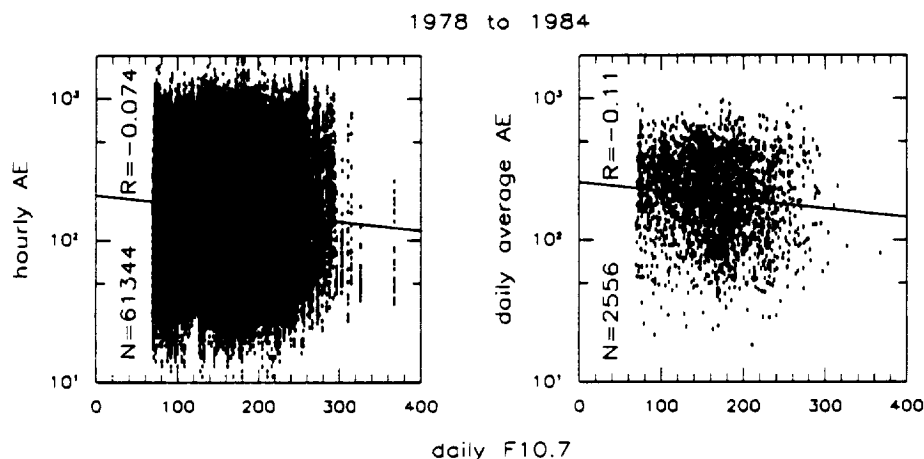

Fig. 9.   Comparison of hourly (Ottawa LT; left) and daily (UT; right) AE indices with the daily solar $F_{10.7}$ index during a 7-year period (year-by-year comparison is made in Table 2).

TABLE 2. Correlation of Log (Hourly AE) With Daily $F_{10.7}$

	Year						
	1978	1979	1980	1981	1982	1983	1984
Number values	8760	8760	8784	8760	8760	8736	8784
Correlation coefficient	0.002	−0.118	0.041	0.074	0.074	0.026	0.065

sheet makes no significant physical difference, but it appears to slightly increase the measurement errors, which is the main reason for keeping the low-energy cutoff at 100 eV/e in this study.

6. CONCLUDING REMARKS

The preceding section makes no mention of the mean energy of the O^+ ions, and there is actually no new information from this study that warrants a discussion beyond what was presented by Lennartsson and Shelley [1986] and Lennartsson [1989]. The only potentially critical issue here is whether the O^+ energy in the central plasma sheet decreases with increasing O^+ density, so as to offset the expected increase in the ion inertial effects. It was found previously that the O^+ mean energy in the 0.1- to 16-keV range is indeed slightly anti-correlated with both geomagnetic [Lennartsson and Shelley, 1986] and solar activity [Lennartsson, 1989], that is anticorrelated with density, but the effect appears far too small to be of any significance here. Specifically, the O^+ mean energy in the central plasma sheet is typically ~4 to 5 keV during low geomagnetic and solar activity and ~3 to 4 keV during moderate to strong activity.

Returning to the far greater variations in the O^+ density, and in the O^+/H^+ density ratio, the challenge is now to interpret their various statistical relations with geomagnetic and solar activity. If one makes the very reasonable assumption that Figures 7 and 8 show a long-term trend that applies also to the central plasma sheet, it is clear that the frequency of occurrence of very large O^+/H^+ ratios in the tail current sheet can be substantially reduced over time with no hindrance to substorms. On the contrary, substorm activity increases. Is this increased activity actually caused by the relative decrease in O^+ content? Considering Figure 5, such a scenario is consonant with the negative correlation between the AE and the $F_{10.7}$ in Figure 9. However, Table 2 shows that this negative correlation, when ordered by calendar year, is not an ordinary feature, but is limited to one (1979) of seven years. This makes it much more likely that the long-term variation of the AE is controlled by a solar process which depends on the solar cycle phase but is not well measured by the $F_{10.7}$, nor by the EUV flux.

Figure 10 may provide additional clues. It appears from Figure 10 that the year 1979 is unique in the sense that the

TABLE 3. ISEE 1 Average Incremental Density From 10- to 100-eV/e Channel in Plasma Sheet

Ion	Increment, %
H^+	2.8
He^{++}	1.3
He^+	8.2
O^+	7.2

AE activity then approaches its absolute minimum in the 7 years considered, a minimum reached in early 1980. Since this occurs while the $F_{10.7}$ is approaching its absolute maximum (Figure 1), it probably accounts for the net negative correlation in Figure 9 (even without the singular $F_{10.7}$ peak in early November 1979). It certainly accounts for the long-term increase in the AE and the Kp in Figures 7 and 8. Whether the early 1980 minimum in the monthly average AE is entirely due to solar processes, or somehow depends on solar-induced changes in the magnetosphere particle populations, it is clearly contrary to having substorm activity enhanced by increased O^+ concentration in the tail current sheet (see also Figure 6).

If there is any significant feedback from the O^+, due to its large ionic mass, it must be negative: The O^+ either inhibits the onset of substorms, acts as a damper on substorms in progress, or helps to release tail stresses at an earlier and "less harmful" stage. However, Figure 10 appears to exclude that scenario as well, since the monthly average AE starts increasing again long (2 years) before the solar $F_{10.7}$ enters its declining phase (Figure 1), which is presumably when the O^+ concentration declines in the plasma sheet (Figure 5).

Short-term correlations are less definitive, for reasons that have been outlined above, but they appear to point in the same direction. Figure 4 suggests that the O^+/H^+ ratio in the plasma sheet does depend on the previous history of the AE, at least over a 2-hour interval (maximum R with two hours delay), but it gives no hint of a similar dependence of the AE on the O^+ concentration, since the correlation in the right panels declines monotonically with time and is anyway much weaker than the autocorrelation of the AE (Table 1). Furthermore, the pattern of scattered points in Figure 4 has an almost triangular shape in the left panels, especially in the bottom panel, with one corner at small ion mass but large AE. This shape implies, ideally, that the AE can take on any large value without O^+ ions being present, and it can do that without increasing the O^+/H^+ ratio uniformly throughout the central plasma sheet, but the O^+/H^+ ratio cannot reach very large values anywhere unless the AE is already large.

6.1. Possible Role of Very Low Energy Ions

Whether the low-energy cutoff is 10 or 100 eV/e, or some intermediate value imposed by positive spacecraft charging, does not appear to make much difference in the central plasma sheet (Table 3), but there may still be a "hidden" ion population with mean energies of a few eV, or less, associated with the terrestrial polar wind and consisting mostly of H^+ ions [e.g., Chappell et al., 1987]. The question is, how large is this polar wind population of H^+ ions compared with the more energetic H^+ population measured on the ISEE 1 spacecraft? Does it have a significant effect on the average ion mass? So far there have been no direct measurements of
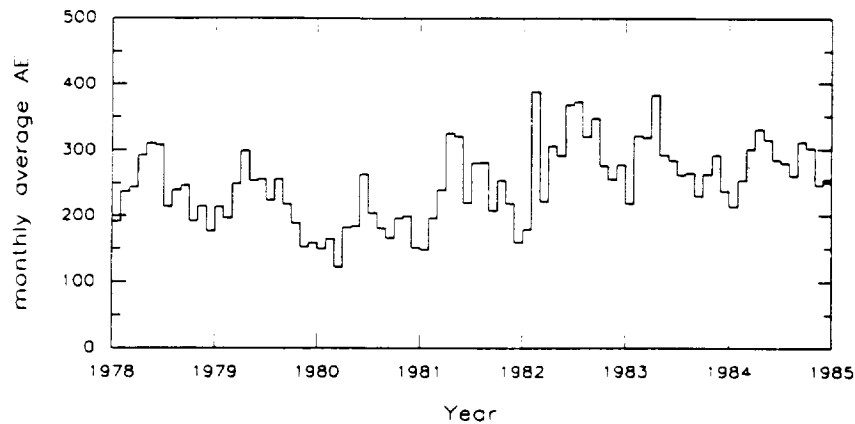
Fig. 10. Long-term variation of monthly averaged AE index (nanoteslas).

ions with only a few eV energy in the plasma sheet, beyond 10 R_E, nor have there been any large-scale attempts to infer "hidden" ions by comparing measured partial ion densities with total electron densities deduced from wave experiments, but the subject has been addressed indirectly by modeling particle trajectories, notably by *Delcourt et al.* [1989].

The numerical model of Delcourt et al. takes into account all presently known sources of terrestrial ion outflows, using the most recent measurements or estimates of source parameters, but it is restricted to radial distances less than 17 R_E, and its plasma sheet does not receive ions whose trajectories intersect the magnetopause or reach beyond 17 R_E downtail. As emphasized by the authors, the trajectory interrupts, especially downtail, set artificial and severe limits on the potential contribution to the plasma sheet density of H⁺ ions with initial energies of 10 eV (cusp source) or greater (auroral zone and polar cap sources) and are the main reason why the calculated H⁺ density between 10 and 17 R_E, including all energies, is only ~0.01 to 0.08 cm⁻³ (Figure 18 in their paper). However, these limits are less severe for the polar wind H⁺ ions, which are all assumed to have an initial energy of only 1 eV, so this model may provide a probable upper limit on their specific contribution in Earth's plasma sheet.

According to Figure 4 in the paper by Delcourt et al., ~43% of the polar wind H⁺ ions remain within the model boundaries during geomagnetically quiet conditions, whereas 41% are lost downtail, because of weak equatorward convection, and 16% are lost at the magnetopause. The 43% that remain are sufficient to dominate the H⁺ density earthward of the 17 R_E boundary, but the density between 10 and 17 R_E is only about 1/10 of the energetic H⁺ density measured on the ISEE 1 (Figure 18 in same paper; see also *Lennartsson and Shelley* [1986]). Fewer of the polar wind ions are lost downtail during disturbed conditions (stronger convection), only ~6%, but the ionospheric source is assumed to be weaker then, by a factor of 2/3 (their Table 2), and a somewhat greater fraction is lost at the magnetopause (23%), so the model H⁺ density in the plasma sheet is still smaller, by a factor of 5 to 10, than the energetic H⁺ density measured on the ISEE 1. Hence, even with all of the lost polar wind H⁺ ions somehow recovered and added to its plasma sheet, this model seems to imply that the density of very low energy H⁺ ions (few eV) is smaller than the known

density of energetic H⁺ ions in Earth's plasma sheet, possibly substantially smaller.

It is worth noting that the polar wind is expected, on theoretical grounds, to be stronger, by approximately a factor of 3, at the minimum of the solar cycle than at the maximum of same [*Chappell et al.*, 1987, and references therein], which is the opposite of the observed long-term trend of the O⁺ flux. To the extent that polar wind H⁺ ions do affect the ion composition in the tail current sheet, they probably amplify the difference in the O⁺/H⁺ ratio between solar maximum and minimum, thereby enhancing the long-term anticorrelation between average ion mass and geomagnetic activity implied by Figures 7 and 8 above.

6.2. Corollary

Since the energetic O⁺ ions do reach the central plasma sheet, well beyond 10 R_E, and do so in sufficient numbers to have a very significant and strongly variable influence on the average mass of keV ions (Figures 4 and 5), they must have significant and variable effects on any tail instability that depends in a decisive fashion on this mass, including any such instability powerful enough to influence the geomagnetic indices. The statistical results of this study suggest therefore that the average ion mass is an unimportant parameter in the equations that govern magnetotail stability. It is clear, at least from the long-term behavior of the AE and Kp indices (Figures 6, 7, 8, and 10), that a more frequent occurrence of large average mass/ion, or mass/charge, in the tail current sheet is not sufficient cause for stronger dissipation of auroral energy. The statistical data are more compatible with reduced energy dissipation when the ion mass becomes extremely large near solar maximum. However, the lack of a consistent correlation over time between solar and geomagnetic indices seems to rule out all significant feedback (Table 2 and Figures 1 and 10). These considerations are nominally based on ion composition data from the 0.1- to 16-keV/e energy range, but probably apply to the bulk of the plasma sheet ions.

REFERENCES

Baker, D. N., E. W. Hones, Jr., D. T. Young, and J. Birn, The possible role of ionospheric oxygen in the initiation and development of plasma sheet instabilities, Geophys. Res. Lett., 9, 1337, 1982.

Baker, D. N., T. A. Fritz, W. Lennartsson, B. Wilken, and H. W. Kroehl, The role of heavy ionospheric ions in the localization of substorm disturbances on 22 March 1979: CDAW-6, J. Geophys. Res., 90, 1273, 1985.

Balsiger, H., P. Eberhardt, J. Geiss, and D. T. Young, Magnetic storm injection of 0.9- to 16-keV/e solar and terrestrial ions into the high altitude magnetosphere, J. Geophys. Res., 85, 1645, 1980.

Bevington, P. R., Data Reduction and Error Analysis for the Physical Sciences, McGraw-Hill, New York, 1969.

Chappell, C. R., T. E. Moore, and J. H. Waite, Jr., The ionosphere as a fully adequate source of plasma for the Earth's magnetosphere, J. Geophys. Res., 92, 5896, 1987.

Daglis, I. A., E. T. Sarris, and G. Kremser, Indications for ionospheric participation in the substorm process from AMPTE/CCE observations, Geophys. Res. Lett., 17, 57, 1990.

Daglis, I. A., E. T. Sarris, and G. Kremser, Ionospheric contribution to the cross-tail current enhancement during the substorm growth phase, J. Atmos. Terr. Phys., 53, 1091, 1991.

Delcourt, D. C., C. R. Chappell, T. E. Moore, and J. H. Waite, Jr., A three-dimensional numerical model of ionospheric plasma in the magnetosphere, J. Geophys. Res., 94, 11,893, 1989.

Ghielmetti, A. G., R. G. Johnson, R. D. Sharp, and E. G. Shelley, The latitudinal, diurnal, and altitudinal distributions of upward flowing energetic ions of ionospheric origin, Geophys. Res. Lett., 5, 59, 1978.

Gloeckler, G., and D. C. Hamilton, AMPTE ion composition results, Phys. Scr., T18, 73, 1987.

Hansen, R. T., S. F. Hansen, and H. G. Loomis, Differential rotation of the solar electron corona, Sol. Phys., 10, 135, 1969.

Hinteregger, H. E., Representations of solar EUV fluxes for aeronomical applications, Adv. Space Res., 1, 39, 1981.

Kamei, T., and H. Maeda, Auroral electrojet indices (AE) for January–June 1978, Data Book 3, World Data Center C2 for Geomagn., Kyoto, Japan, April 1981.

Kremser, G., W. Stüdeman, B. Wilken, G. Gloeckler, D. C. Hamilton, and F. M. Ipavich, Observations of energetic oxygen and carbon ions with charge states between 3 and 6 in the magnetosphere, Ann. Geophys., 6, 325, 1988.

Lennartsson, W., Energetic (0.1–16 keV/e) magnetospheric ion composition at different levels of solar F10.7, J. Geophys. Res., 94, 3600, 1989.

Lennartsson, W., and R. D. Sharp, A comparison of the 0.1–17 keV/e ion composition in the near equatorial magnetosphere between quiet and disturbed conditions, J. Geophys. Res., 87, 6109, 1982.

Lennartsson, W., and E. G. Shelley, Survey of 0.1- to 16-keV/e plasma sheet ion composition, J. Geophys. Res., 91, 3061, 1986.

Lundin, R., B. Hultqvist, N. Pissarenko, and A. Zakharov, The plasma mantle: Composition and other characteristics as ob-

served by means of the Prognoz-7 satellite, Space Sci. Rev., 31, 247, 1982.

Möbius, E., M. Scholer, B. Klecker, D. Hovestadt, G. Gloeckler, and F. M. Ipavich, Acceleration of ions of ionospheric origin in the plasma sheet during substorm activity, in Magnetotail Physics, edited by A. T. Y. Lui, Johns Hopkins University Press, Baltimore, 231, 1987.

Moore, T. E., and D. C. Delcourt, Transport and energization of ionospheric plasma (abstract), EOS Trans. AGU, 73(43), Fall Meeting suppl., 471, 1992.

Mozer, F. S., E. W. Hones, Jr., and J. Birn, Comparison of spherical double probe electric field measurements with plasma bulk flows in plasmas having densities less than 1 cm⁻³, Geophys. Res. Lett., 10, 737, 1983.

Peterson, W. K., R. D. Sharp, E. G. Shelley, and R. G. Johnson, Energetic ion composition of the plasma sheet, J. Geophys. Res., 86, 761, 1981.

Potemra, T. A., L. J. Zanetti, and M. H. Acuña, The AMPTE CCE Magnetic Field Experiment, IEEE Trans. Geosci. Remote Sens., GE-23, 246, 1985.

Press, W. H., B. P. Flannery, S. A. Teukolsky, and W. T. Vetterling, Numerical Recipes, Cambridge University Press, New York, 1986.

Russell, C. T., The ISEE 1 and 2 fluxgate magnetometers, IEEE Trans. Geosci. Electron., GE-16, 239, 1978.

Sharp, R. D., D. L. Carr, W. K. Peterson, and E. G. Shelley, Ion streams in the magnetotail, J. Geophys. Res., 86, 4639, 1981.

Shelley, E. G., R. G. Johnson, and R. D. Sharp, Satellite observations of energetic heavy ions during a geomagnetic storm, J. Geophys. Res., 77, 6104, 1972.

Shelley, E. G., R. D. Sharp, R. G. Johnson, J. Geiss, P. Eberhardt, H. Balsiger, G. Haerendel, and H. Rosenbauer, Plasma composition experiment on ISEE-A, IEEE Trans. Geosci. Electron., GE-16, 266, 1978.

Shelley, E. G., A. Ghielmetti, E. Hertzberg, S. J. Battel, K. Altwegg-Von Burg, and H. Balsiger, The AMPTE CCE Hot Plasma Composition Experiment (HPCE), IEEE Trans. Geosci. Remote Sens., GE-23, 241, 1985.

Singer, H. J., C. T. Russell, M. G. Kivelson, T. A. Fritz, and W. Lennartsson, Satellite observations of the spatial extent and structure of PC 3, 4, 5 pulsations near the magnetospheric equator, Geophys. Res. Lett., 6, 889, 1979.

Strangeway, R. J., and R. G. Johnson, Energetic ion mass composition as observed at near-geosynchronous and low altitudes during the storm period of February 21 and 22, 1979, J. Geophys. Res., 89, 8919, 1984.

Swift, D. W., The role of ionospheric plasma in substorm models (abstract), Eos Trans. AGU, 73(43), Fall Meeting suppl., 472, 1992.

Yau, A. W., E. G. Shelley, W. K. Peterson, and L. Lenchyshyn, Energetic auroral and polar ion outflow at DE 1 altitudes: Magnitude, composition, magnetic activity dependence, and long-term variations, J. Geophys. Res., 90, 8417, 1985.

Young, D. T., H. Balsiger, and J. Geiss, Correlations of magnetospheric ion composition with geomagnetic and solar activity, J. Geophys. Res., 87, 9077, 1982.

D. M. Klumpar, O. W. Lennartsson, J. M. Quinn, and E. G. Shelley, Lockheed Missiles and Space Company, Inc., Research and Development, Dept. 91-20, Bldg. 255, 3251 Hanover Street, Palo Alto, CA 94304.

REPORT DOCUMENTATION PAGE

Form Approved
OMB No 0704 0188

1. AGENCY USE ONLY *(Leave blank)*	2. REPORT DATE 4/20/94	3. REPORT TYPE AND DATES COVERED Final Report, 10 Apr 91 – 9 May 94

4. TITLE AND SUBTITLE

A STUDY OF THE FORMATION AND DYNAMICS OF THE EARTH's

PLASMA SHEET USING ION COMPOSITION DATA

5. FUNDING NUMBERS

C: NAS5-31209

6. AUTHOR(S)

O. W. Lennartsson, Principal Investigator

7. PERFORMING ORGANIZATION NAME(S) AND ADDRESS(ES)

Lockheed Missiles & Space Company, Inc.
Research and Development Division
0/91-20, B/255, Fac. 2
3251 Hanover Street
Palo Alto, CA 94304-1187

8. PERFORMING ORGANIZATION REPORT NUMBER

F254278

9. SPONSORING/MONITORING AGENCY NAME(S) AND ADDRESS(ES)

NASA/ Goddard Space Flight Center
Greenbelt, Maryland 20771
Technical Officer: G. D. Bullock, Code 602

10. SPONSORING/MONITORING AGENCY REPORT NUMBER

11. SUPPLEMENTARY NOTES

12a. DISTRIBUTION/AVAILABILITY STATEMENT

Unlimited/ Unclassified

12b. DISTRIBUTION CODE

13. ABSTRACT *(Maximum 200 words)*

Over two years of data from the Lockheed Plasma Composition Experiment on the ISEE 1 spacecraft, covering ion energies beween 100 eV/e and about 16 keV/e, have been analyzed in an attempt to extract new information about three geophysical issues: (1) solar wind penetration of Earth's magnetic tail, (2) relationship between plasma sheet and tail lobe ion composition, and (3) possible effects of heavy terrestrial ions on plasma sheet stability.

The results suggest: (1) The solar wind enters the magnetic tail at all times along slots between the plasma sheet and tail lobes, convected inward by the electric fringe field of the low-latitude magnetopause boundary layer. (2) The density gradient between the plasma sheet and the tail lobes is the steepest for protons, and becomes gradually smoother with increasing ionic mass, possibly associated with the different characteristic gyroradii. (3) The energetic singly charged oxygen ions of terrestrial origin do not have a significant effect on the stability of the plasma sheet, in spite of the fact that they often contribute most of the ion mass density inside of the ISEE 1 apogee near 23 earth radii downtail.

14. SUBJECT TERMS

Ion Composition, Magnetotail, Plasma Sheet, Tail Lobes,
Solar Wind Entry, Energetic Ions, Ion Flows, Current Sheet

15. NUMBER OF PAGES

76

16. PRICE CODE

17. SECURITY CLASSIFICATION OF REPORT	18. SECURITY CLASSIFICATION OF THIS PAGE	19. SECURITY CLASSIFICATION OF ABSTRACT	20. LIMITATION OF ABSTRACT
Unclassified	Unclassified	Unclassified	Unlimited

GENERAL INSTRUCTIONS FOR COMPLETING SF 298

The Report Documentation Page (RDP) is used in announcing and cataloging reports. It is important that this information be consistent with the rest of the report, particularly the cover and title page. Instructions for filling in each block of the form follow. It is important to *stay within the lines* to meet *optical scanning requirements*.

Block 1. Agency Use Only *(Leave blank)*.

Block 2. Report Date. Full publication date including day, month, and year, if available (e.g. 1 Jan 88). Must cite at least the year.

Block 3. Type of Report and Dates Covered. State whether report is interim, final, etc. If applicable, enter inclusive report dates (e.g. 10 Jun 87 - 30 Jun 88).

Block 4. Title and Subtitle. A title is taken from the part of the report that provides the most meaningful and complete information. When a report is prepared in more than one volume, repeat the primary title, add volume number, and include subtitle for the specific volume. On classified documents enter the title classification in parentheses.

Block 5. Funding Numbers. To include contract and grant numbers; may include program element number(s), project number(s), task number(s), and work unit number(s). Use the following labels:

C	-	Contract	PR	-	Project
G	-	Grant	TA	-	Task
PE	-	Program Element	WU	-	Work Unit Accession No.

Block 6. Author(s). Name(s) of person(s) responsible for writing the report, performing the research, or credited with the content of the report. If editor or compiler, this should follow the name(s).

Block 7. Performing Organization Name(s) and Address(es). Self-explanatory.

Block 8. Performing Organization Report Number. Enter the unique alphanumeric report number(s) assigned by the organization performing the report.

Block 9. Sponsoring/Monitoring Agency Name(s) and Address(es). Self-explanatory.

Block 10. Sponsoring/Monitoring Agency Report Number. *(If known)*

Block 11. Supplementary Notes. Enter information not included elsewhere such as: Prepared in cooperation with...; Trans. of...; To be published in.... When a report is revised, include a statement whether the new report supersedes or supplements the older report.

Block 12a. Distribution/Availability Statement. Denotes public availability or limitations. Cite any availability to the public. Enter additional limitations or special markings in all capitals (e.g. NOFORN, REL, ITAR).

- **DOD** - See DoDD 5230.24, "Distribution Statements on Technical Documents."
- **DOE** - See authorities.
- **NASA** - See Handbook NHB 2200.2.
- **NTIS** - Leave blank.

Block 12b. Distribution Code.

- **DOD** - Leave blank.
- **DOE** - Enter DOE distribution categories from the Standard Distribution for Unclassified Scientific and Technical Reports.
- **NASA** - Leave blank.
- **NTIS** - Leave blank.

Block 13. Abstract. Include a brief *(Maximum 200 words)* factual summary of the most significant information contained in the report.

Block 14. Subject Terms. Keywords or phrases identifying major subjects in the report.

Block 15. Number of Pages. Enter the total number of pages.

Block 16. Price Code. Enter appropriate price code *(NTIS only)*.

Blocks 17. - 19. Security Classifications. Self-explanatory. Enter U.S. Security Classification in accordance with U.S. Security Regulations (i.e., UNCLASSIFIED). If form contains classified information, stamp classification on the top and bottom of the page.

Block 20. Limitation of Abstract. This block must be completed to assign a limitation to the abstract. Enter either UL (unlimited) or SAR (same as report). An entry in this block is necessary if the abstract is to be limited. If blank, the abstract is assumed to be unlimited.